DUAL HOT WIRE PROBES WITHOUT CROSSED PRONG-WIRE INTERFERENCE EFFECTS

Argüelles Díaz, Katia María
University of Oviedo, Fluid Dynamics Group
Viesques, 33271, Gijón (Asturias), Spain
arguelleskatia@uniovi.es

Fernández Oro, Jesús Manuel
University of Oviedo, Fluid Dynamics Group
Viesques, 33271, Gijón (Asturias), Spain
jesusfo@uniovi.es

Galdo Vega, Mónica
University of Oviedo, Fluid Dynamics Group
Viesques, 33271, Gijón (Asturias), Spain
galdomonica@uniovi.es

Blanco Marigorta, Eduardo
University of Oviedo, Fluid Dynamics Group
Viesques, 33271, Gijón (Asturias), Spain
eblanco@uniovi.es

ABSTRACT

Dual Hot Wire (DHW) probes are widely used for the measurement of two-dimensional velocity flows. Typically, the two wires of this kind of probes are placed either orthogonal or with a larger angle between them (i.e. 120º) in order to increase the measurement angular range of the probe. For both orthogonal and non-orthogonal probes, certain angular ranges of the incident flow imply that the inner wire is found in the wake of one of the prongs of the outer wire, causing significant interference effects and a practical limitation of the measurement angular range of the probes. This angular range may be insufficient when trying to measure flows with sudden and notable changes of direction. This work proposes new designs of DHW probes without cross prong-wire interference effects for a significant angular interval. As a consequence, the measurement angular range of these enhanced probes is significantly extended, allowing a reliable determination of flows with important recirculation effects, such as those found in turbomachinery environments.

INTRODUCTION

Thermal anemometry is a measuring technique that retrieves the flow velocity through heat transfer variations in a small sensor that it is electrically heated while exposed to a moving fluid. It is a reliable method, extremely accurate and with a high frequency response.

The most common thermal anemometer is the hot wire thermal device, which it is composed by a single or multiple tiny wires mounted on the probe tip. Tungsten is typically considered as the wire material due to its electrical resistance which is particularly suitable to be heated under regular values of intensity or voltage. Every wire is weld to a couple of prongs, usually of stainless steel, incrusted to the probe support, which are also employed as electrical contacts to heat the wire to a temperature in the range of 200-300 ºC.

Wire's diameter must be extremely reduced so the signal-to-noise ratio at high frequencies may be amplified, the spatial resolution and frequency response increased, and the heat conduction losses and interferences with the flow minimized. Additionally, the diameter size must be large enough to increase the wire resistance and reduce aging effects provoked by particles transported by the flow. It is accepted that optimal wire diameters must be ranged between 2 to 5 μm, resulting in extremely low Reynolds numbers which lead to consider the incident flow over the wires as symmetric and quasi-steady.

On the other hand, the wire's length must be also quite reduced to enlarge the probe's spatial resolution and minimize the aerodynamic load, while keeping a minimum size to control conduction losses and preserve a uniform temperature distribution. Optimal values are found when the length-to-diameter ratio is about 200 ([1]), although it must be kept in mind that the spatial resolution is also conditioned by the existing distance between the wires ([2]).

When the flow impinges on a hot wire, part of its heat energy is advected by the flow (forced convection [3]) due to the relative difference between the temperatures of the sensor (hot) and the fluid flow (cold). Because of the wire thermal inertia, its frequency response to flow velocity variations is dumped, so the final measured changes in voltage turn to be lesser than the real ones. As a consequence, the wire self-response is excessively low and needs to be electronically compensated using, for instance, a constant temperature anemometer (CTA). This kind of equipment is an amplifier device that feeds back the wires to maintain its temperature independent of the variations in the flow velocity ([4]). Using this technique, the frequency limit can be significantly raised, up to 1000 times higher ([5], [6]).

Every probe must be calibrated before it can be used to measure a particular flow. The calibration determines a relationship between the output voltage of every single wire and the magnitude and direction of the flow velocity vector. The electrical current in the wires provokes a heat release that must be transferred to the surrounding fluid to restore the thermodynamic equilibrium. If the flow velocity is modified, then the heat transfer changes so the wire temperature must evolve until a new equilibrium situation is reached. The heat transfer rate is directly related to the flow velocity impinging on the sensor. The feedback control of the CTA acts to modify the intensity of the electrical current so the wire temperature remains constant overtime. Consequently, the flow velocity can be determined through the measurement of the intensity or voltage modifications needed to keep the wire at constant temperature.

The most popular method to calibrate hot wire probes consists in keeping them steadily in a moving fluid. This calibration, known as "static calibration", is completed in a two-step sequence. In the first one, the probe is located in the calibration facility, with both yaw and pitch angles set to zero, so one can obtain the relationship between the effective velocity in every wire and the CTA output voltage, including a correction factor for the temperature difference. Such relationship is given by the well-known King's law ([7]) and represents the transfer function to be used when transforming voltage data into flow velocities. The second step is to complete the angular calibration, required for two and three-wire probes, to determine its directional sensitivity, that is, the relationship between the effective voltage and the components of the velocity field. Such relationship can be approximated via analytical functions, or can be obtained by means of a direct calibration procedure, which comprises the derivation of three coefficients to represent the flow angle and the change in velocity magnitude ([8]-[10]). For that purposes, the pitch angle is set to zero while the yaw angle is ranged from a minimum to a maximum value, obtaining the value of the calibration coefficients for every angular position. Thus, the resulting distributions are employed instead of the analytical functions, giving more precise results because all the geometrical effects and manufacturing imperfections are considered inherently.

Ref. [11] describes in detail a direct calibration procedure for a three-wire probe, including the uncertainty transmitted to the measurements; while references [12] and [13] provide an in-depth review of the different calibration methods available for hot wire probes.

Using dual hot wire (DHW) probes, we can obtain in-plane velocity components of the flow. The most common configuration is the so-called X-probe, consisting in a hot wire anemometer with two crossed wires, either in an orthogonal or a non-orthogonal disposition. If the wires are orthogonal to each other, the maximum angular range cannot exceed 90 deg, while higher angle between the wires (i.e. 120 deg) may provide and extended angular range ([14], [15]). Anyway, whatever the angle selected, if the X-probes are built with the supporting prongs in a perpendicular orientation respect to the measuring plane (figure 1a), there are certain angular positions where interference effects between the first wire and the prongs of the second wire arise. These effects are superimposed to the self interference of one wire with its own prongs, which is clearly less important than crossed interferences ([16]).

The crossed interference effect appears for certain yaw angles when one of the probe's wires is found in the wake of a prong of the other wire. This effect, which has been already identified and studied by several authors ([17], [18]), can be called as "wake interference effect", and implies that the wire affected by the prong wake (i.e. in a region with a notable velocity deficit) is measuring flow velocities significantly lower than those of the real flow. The direct consequence is a reduction in the measuring angular range of the probe. Furthermore, it is expected the appearance of an artificial induced turbulence which may limit the wire frequency response and affect negatively the accuracy of the velocity measurements. Concerning this point, it is possible that if the velocity to be measured differs significantly respect to the calibration conditions, this effect could lead to a considerable error in the final measurements.

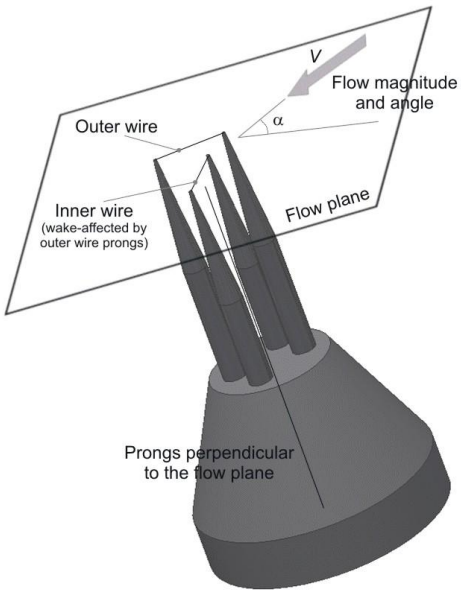

Fig. 1a. Typical 120 deg, non-orthogonal X-type DHW probe with prong-wire interference.

Fig. 1b. 120 deg, Z-type DHW probe without wake interference effects.

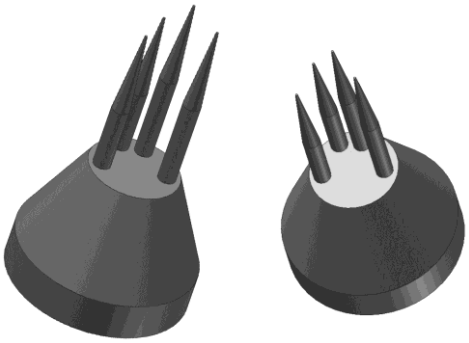

Fig. 1c. 120 deg, V-type DHW probe without wake interference effects.

To overcome these problems, the probes can be designed with the supporting prongs placed in a plane parallel to the one of the incident flow. Hence, the wake interference effect vanishes, remaining exclusively the interference effect of the wires with their own prongs, and increasing the angular range accordingly. A wide catalog of commercial designs for DHW probes with or without wake interference effects can be found in the technical literature. As an example, figure 2 shows some of these designs from leading manufacturers of hot wire probes like DANTEC and TSI.

For the present investigation dealing with interference effects, two DHW probes have been built, denoted as Z-type and V-type, with the wire prongs placed in a parallel plane to the flow pattern (figure 1b and 1c respectively). These probes have been calibrated in an aerodynamic calibration facility and compared with the results obtained for a classic 120 deg X-type probe. It is found that both Z-type and V-type calibrations are similar (for probes with identical geometrical characteristics in terms of wires diameter, wires lengths and overall probe size), presenting accurate calibration coefficients without severe interference irregularities.

Following sections present the conclusions obtained in terms of accuracy gained with free-wake interference probes. Both angular ranges and influences of the Reynolds number, as well as turbulence levels, are explored in order to provide a comprehensive overview of the interference impact over those parameters for developers and users of hot-wire measuring devices.

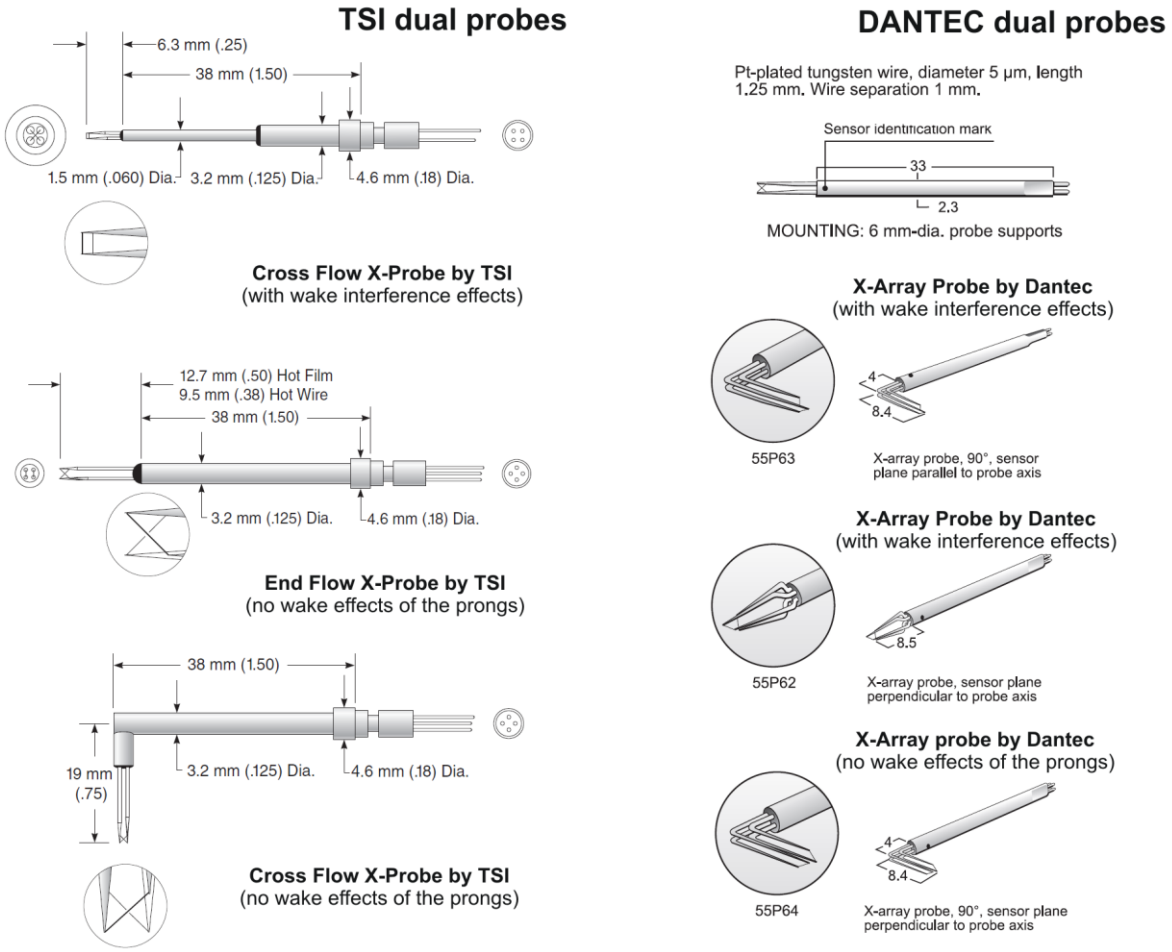

Fig. 2. Commercial designs of DHW anemometers by leading manufacturers TSI and Dantec.

PROBES GEOMETRY AND EXPERIMENTAL SETUP

Three different probe geometries have been considered for the present investigation. The original design is a classical X-type probe with the supporting prongs perpendicular to the flow plane. This means that the inner wire suffers wake interferences coming from the prongs of the outer wire. The remaining probes, designated as Z-type and V-type probes, are improved versions developed to eliminate interference effects, with the prongs placed in a plane parallel to the flow. All the probes were in-home manufactured, with tungsten wires of 5 µm and 1 mm long, in a 120 deg crossed arrangement. The wire prongs are stainless steel needles with 0.4 mm diameter. Figure 1 presents a schematic view of the geometrical characteristics of the probes.

Both Z-type and V-type probes should present analogous calibration coefficients and similar measurements results. For practical reasons, we have employed intensively the V-type probe for the experimental characterization of flow fields due to its higher compactness and simplicity to be manufactured or repaired.

The calibration facility is an opened nozzle with a circular discharge section of 1.5 cm dia. This nozzle supplies a uniform incident flow over the hot-wire probes when mounted in the test section. The flow rate can be regulated with a throttling valve placed on the compressed air supply, so the velocity can be ranged from 0 to 70 m/s approximately.

The probes are typically placed 20 mm downstream of the nozzle discharge, aligned with the jet axis. For a fixed angular position, the velocity is progressively increased from zero to the maximum velocity, obtaining the King's law for every wire. One single wire can only measure the normal velocity component, which is usually

known as effective velocity. When probes with more than one unique wire are employed, the proximity between the different wires and the supporting prongs provokes that effective velocities of the wires differ from the case when every wire is isolated. This is traduced in the need for an additional angular calibration, changing the incidence angle of the calibration flow for a fixed velocity magnitude. This angular repositioning is carried out by means of a two-axis mechanical gear, driven by a couple of step-by-step motors controlled via PC. For two-wire anemometers, only one axis rotation is needed (yaw angle), while three-wire probes require both yaw and pitch angles relocations. Finally, the effective velocity of every wire is monitored as a function of the flow angle and the angular calibration coefficients of the probe are determined to complete the procedure.

During the calibration, the probe wires are connected to a four channel, TSI IFA-100, CTA anemometer. The measured data is acquired with a NIDAQ PCI device, 16-bit A/D converter, which are following stored in a PC using MATLAB routines and specific libraries. For every measuring point, up to 10^4 samples, at a low-frequency response of 100 Hz, are recorded. The surrounding environmental conditions of the calibration facility are controlled and the temperature variations within the calibration room are also registered. Additionally, calibration measurements have been also conducted modifying the inlet turbulence of the incident flow (with a perturbing grid mounted on the nozzle) to analyze the impact of this additional parameter on the wake interference effect.

RESULTS AND DISCUSSION

A direct calibration procedure ([11]) has been applied with these three DHW probes, ad hoc manufactured in the Fluid Mechanics Lab of the School of Engineering at the University of Oviedo, to confirm the characteristics explained above. For every probe, the King's law has been experimentally determined, and the angular calibration for a reference velocity has been completed. Finally, an angular calibration coefficient has been defined from the output voltage of the wires as follows:

$$\text{Acf} = U_{e1} - U_{e2} \tag{1}$$

where U_{e1} y U_{e2} correspond to the effective velocities of both external (wire 1) and internal (wire 2) wires.

Calibration distributions of the X-type probe (with wake interference effects)

Figure 3 shows angular distributions of the output signals (in voltage) in the wires, obtained during calibration. Though not shown here, an angular discretization of 2.5 deg has been chosen for the entire data sets, which has been found accurate enough to determine the angular variations.

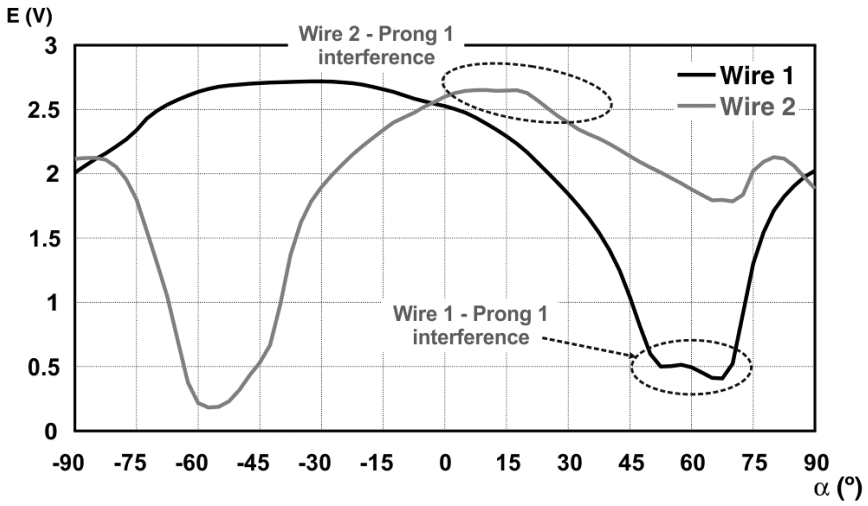

Fig. 3: Angular distributions of wires output voltage for a 120 deg DHW X-probe.

Interference effects between the wires and their own prongs or between the wires and the wake fluid coming from adjacent prongs are manifested as oscillations in the output signals of the probe. Such perturbations may lead to the appearance of two different detrimental effects. In the one hand, they can induce the arising of double points in the distribution of the angular calibration, which implies the impossibility for a unique determination of the angle and a practical reduction in the operative angular range of the probe. On the other hand, if the flow angle to be measured is placed within the angular interval of the calibration affected by interference effects, the measurement accuracy drops severely and consequently the error in the determination of the velocity and flow angle increases.

In the case of the present X-type probe, the wire interference with their own prongs appears when the incident flow angle is high. In particular, wire 1 suffers self-interference between 50 and 70 deg (see annotations in fig. 3); while wake interferences are observed earlier exclusively in the second wire (the inner wire) for small yaw angles. In this case this effect modifies the probe performance for the angular interval between 0 and 30 deg, being maximum at 20 deg approximately.

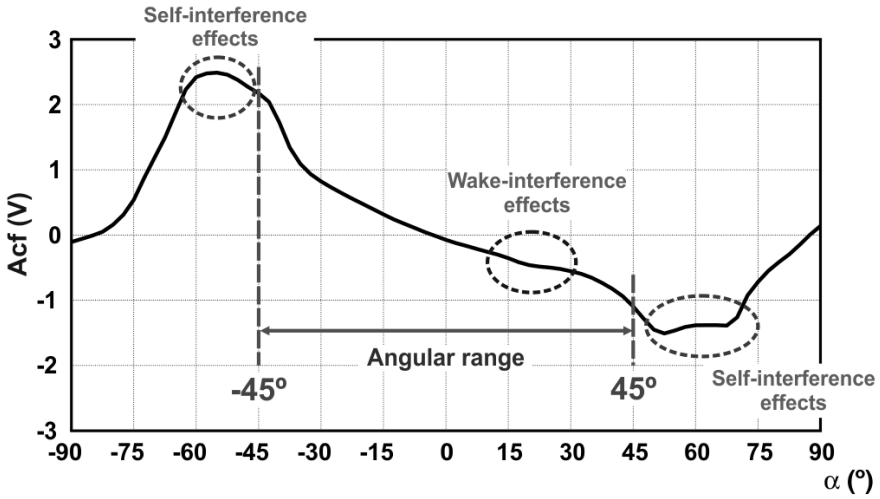

Fig. 4: Angular coefficient for a 120 deg DHW X-probe.

Figure 4 shows the angular coefficient of the X-type probe, in terms of output voltage, obtained using equation 1. The overall angular range of the probe turns to be 90 deg, being operative for angular measurements between -45 and 45 deg. Note that in this case, the limits of the angular range are established by the self-interference effects of the wires with their own prongs. The wake-interference effect is manifested as a perturbation in the angular coefficient at 20 deg, which will surely lead to a lower precision of the flow measurements for flow angles in that zone. Moreover, it is expected that irregularity in the angular calibration could lead in practice to a further reduction of the angular range to the (-45, 0) deg interval. Depending on the application, this angular range can be not sufficient to describe flow angle variations overtime.

The appearance of wake interference effects for positive flow angles close to 0 deg is due to the equal length of the wires in the X-type design. Hence, when misalignment of the yaw angle towards positive values comes across, the inner wire is automatically placed in the wake of a prong of the outer wire. This characteristic can be retarded if the probe wires are built with different lengths, so the outer wire is made larger than the inner one. Figure 5 shows how the wake effect is effectively displaced towards higher yaw angles with non-equal wires.

Precisely, such a figure represents the wires output signals and the corresponding angular calibration for X-type probes with wires of different length. Note that self-interference of a wire with its own prong is more pronounced for the second wire than for the first one, because it results to be shorter due to the 120 deg X-type design. These interference effects are manifested at -58 deg and 110 deg approximately for wire 2, and only at -110 deg for wire 1. As expected, the wake interference effect is only experienced in the inner wire, as a consequence of the deficit velocity induced by the outer wire prongs for yaw angles ranged between 30 and 65 deg.

The wake interference effect is now fixed as the limitation for positive values of the angular range, so the operative zone of the angular calibration (88 deg) is established between -58 and 30 deg. Due to the wires asymmetry, the wake interference is now more severe (see the wore response marked with a dashed oval in the figure) and turns to be a real limit for the angular calibration; but on the contrary, it has been possible to extend the practical angular range from 45 to 88 deg.

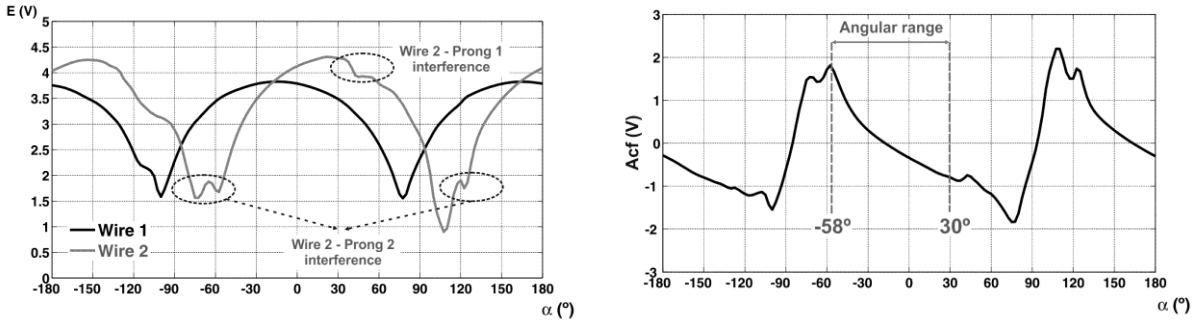

Fig. 5: Angular distributions of wires output voltage and angular calibration coefficient for a 120 deg DHW X-probe with different length wires.

In order to study how wake interference impact have a detrimental effect on the measurements accuracy, several tests with the classic X-type probe of equal length wires have been conducted. For that purpose, the starting point has been the determination of the angular calibration for an averaged incident flow velocity of 40 m/s, already reported in figures 3 and 4.

After calibration, the tests facility is employed for measurements acquisition. In particular, measurements have been performed for several flow velocities (differing from the calibration conditions) ranging from 20 to 60 m/s at intervals of 10 m/s. Additionally, for every Reynolds number, we have gone through a wide number of angular positions including free-wake positions and also locations susceptible of wake interference. The incidence flow angle has been ranged from -40 to 40 deg in a 10 deg interval between consecutive positions.

Error in the determination of the velocity magnitude with the X-type probe

Figure 6 represents the error associated to flow velocity retrievement when the 40 m/s calibration is employed to reduce data coming from measurements taken at other flow velocities. The error is expressed in a percentage basis according to the following formula:

$$\text{Velocity error} = 100 \times \frac{\left| V_{real} - V_{measurement} \right|}{V_{real}} \tag{2}$$

where $v_{measurement}$ is the velocity registered with the hot-wire probe and v_{real} is the real velocity magnitude measured by means of a pressure transducer connected to the NIDAQ acquiring card in the nozzle discharge.

The results have been split in two different figures for clarity. Figure 6a shows the error distributions corresponding to flow angles for -40 to 0 deg out of the wake-affected region (in this case, negative yaw angles). It is observed how the errors in velocity are increased as the incident flow angles are closer to the limits of the angular calibration. For 40 m/s incident flow, the error is minimum at 0 deg (around 1%) and maximum at extreme -40 deg (around 4%).

As expected, the errors are also intensified as the incident flow velocity is progressively separated from calibration conditions. All the angular positions present their relative minimum at 40 m/s, revealing the overall coherency of the present data set. Also, it is observed a slight trend to obtain higher error for lower velocities than for higher velocities respect to the calibration reference. In particular, all the flow angles present their maximum errors around a significant 12%, at 20 m/s.

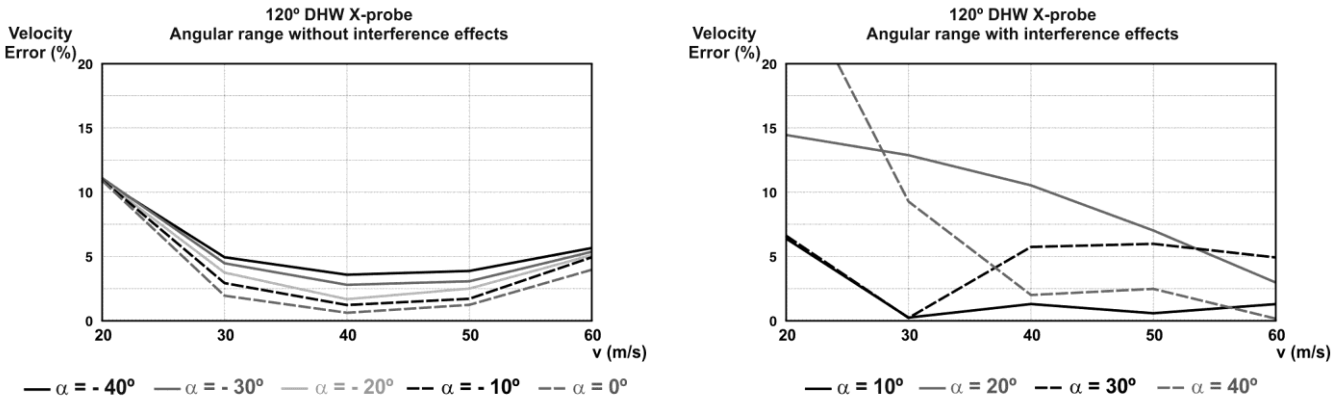

Fig. 6. Error associated to the determination of the velocity magnitude at different operating conditions. a) zone without wake interferences; b) zone with wake interferences.

Figure 6b reveals analogous results now for flow angles between 10 and 40 deg within the wake-affected region. First of all, the error evolution is not as clear as in previous figure 6a. The minimum values are no longer obtained at 40 m/s, but it can be reasonably accepted a similar trend than before with higher errors for lower velocities. Additionally, the error is generally the largest for 20 deg angular positions, where the wake interference effect is maximum.

The conclusion from results shown in figure 6b is that when an incident flow angle is measured with the probe working under wake-interference conditions, the error involved in the determination of the velocity magnitude is excessive to validate that intermediate angular interval, so the operative range has to be limited to the free-wake regions as previously warned.

Error in the determination of the flow angle with the X-type probe

Following, similar considerations for the flow angle determination are presented below. Now, the error in the angle retrievement when measuring for Reynolds numbers out of the calibration conditions is calculated according to:

$$\text{Flow Angle Error} = \left|\alpha_{real} - \alpha_{measurement}\right| \tag{3}$$

where $\alpha_{measurement}$ represents the flow angle retrieved with the X-type probe and α_{real} corresponds to real misalignment of the probe, respect to the incident jet, determined from the repositioning system of the calibration facility (step-by-step motor) and confirmed with a goniometer.

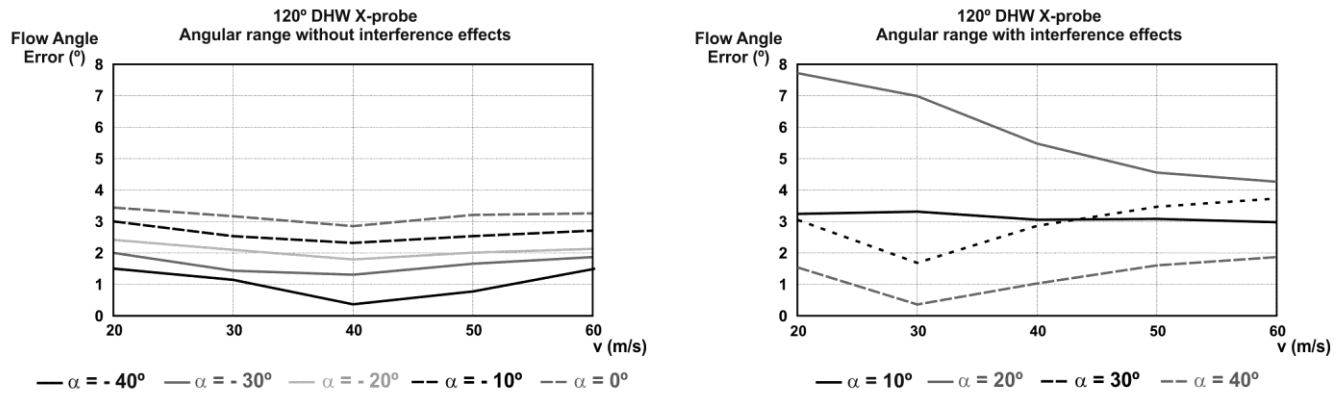

Fig. 7. Error associated to the determination of the flow angle at different operating conditions. a) zone without wake interferences; b) zone with wake interferences.

In a similar fashion, the results are shown in two complementary figures (7a and 7b). Figure 7a includes the results from free-wake angular zones. Now, the general trend is opposite to the one analyzed in figure 6a, so the error associated to the flow angle retrievement turns to be higher for yaw angles close to 0 deg, being progressively reduced as we move towards the angular limits of the calibration (-40 deg). Typical errors are found to be of 3 deg at $\alpha=0^o$ and 1 deg at $\alpha=-40^o$. On the contrary, concerning discrepancies in the flow velocity respect to calibration conditions, relative minima appear once again at 40 m/s, with similar deviation at both high and low velocities (note that error distributions as a function of the yaw angle seem to be quite constant for the whole of velocities tested).

To conclude this section, figure 7b completes the analysis with results from the wake-affected region. As in previous figure 6b, no clear trend can be derived from the obtained distributions. When the yaw angle is set to 10 deg (black solid line), the error is almost constant (around 3 deg), whatever incident flow velocity considered. In the case of $\alpha=30^o$ and $\alpha=40^o$, the error in angle is minimum at 30 m/s and maximum at 60 m/s. Alternatively, for the angle with the maximum wake interference ($\alpha=20^o$), the error is progressively increased as the flow velocity slows down with the maximum error reaching 7.5 deg. Also note that for this particular angle, the errors are notably higher than any other angle considered.

All these considerations confirm, also for the flow angle retrievement, that X-type probes should not be operated when the incident flow angle induces wake interference effects on the wires.

Wake interference effect on the determination of turbulence intensities with the X-type probe

Additionally, the impact of measuring with the X-type probe in the wake-affected region of the calibration has been analyzed in terms of turbulence prediction. Notice that when wake interference effects are perturbing the inner wire, there must be superimposed an additional, fictitious turbulence provoked by the vortex shedding of the outer prongs, that may lead to an overestimation in the quantification of real flow turbulence levels.

In order to study such hypothesis, additional tests at full high-frequency response of the X-type probe have been conducted. In particular, every measuring point has been sampled at 30 kHz (close to the maximum frequency response of the probe), recording 10000 instantaneous values during 0.3 seconds. Two different datasets have been considered for the analysis. Firstly, measuring in an incident flow with identical levels of inlet turbulence to those experienced during calibration (denoted as free-stream turbulence). Secondly, placing the probe in a flow with a slightly higher inlet turbulence (denoted as grid turbulence), which has been generated with a perturbing grid at the nozzle discharge of the facility. Measurements for impinging velocities of 30, 40 and 50 m/s have been performed in both settings, ranging the yaw angle of the probe from -40 to 40 deg in a 10 deg interval. The angular calibration at 40 m/s has been systematically applied for data reduction of all the measured points.

Figure 8 shows power spectra of the time series corresponding for measurements obtained at 0 yaw angle (no interference with outer prongs) and 30 deg yaw angle (wake affected region) for an incident velocity of 40 m/s. Since they have been derived with the 40 m/s calibration, they are free of inaccuracies related to Reynolds number deviations. Upper plot includes results from free-stream turbulence condition, while lower plot reproduces similar results for grid turbulence database. Both figures represent in the y-axis, in a logarithmic scale, the power spectrum density (PSD) of the axial velocity fluctuation from the instantaneous traces. These spectra have been post-processed with a smoothed periodogram based on a parametric algorithm (autoregressive 800th order) in order to reduce spurious scatter. Additionally, a high-pass filter of 300 Hz has been used for signal conditioning to eliminate low-frequency oscillations of the supplying compressed air.

Both situations (free-stream and grid turbulence) reveal that the energetic contents corresponding to wake-affected regions (30 deg) are higher for all the turbulent scales (throughout the whole frequency range) than out-of-wake locations (0 deg), clearly indicating that the probe is measuring an overestimated turbulence intensity at 30 deg yaw angle. It is also remarkable that for those spectra corresponding to free-stream conditions (figure 8a), there is a peak of turbulent kinetic energy around 1 kHz for all the angular ranges tested. This phenomenon is reproduced for all the different velocities analyzed, as it can be seen in the small plot of the lower left corner in the figure. Note that this frequency signature is shifted along the x-axis as the mean incident velocity is increased. The linear displacement observed indicates that this phenomenon must be related to vortex shedding in the nozzle discharge because when the grid is installed, this effect is vanished. In particular, considering a

typical Strouhal number around 0.2, it has been estimated a 7 mm length scale as representative for vortex shedding, in reasonable accordance with the real blunt thickness of the nozzle endwall at the calibration facility.

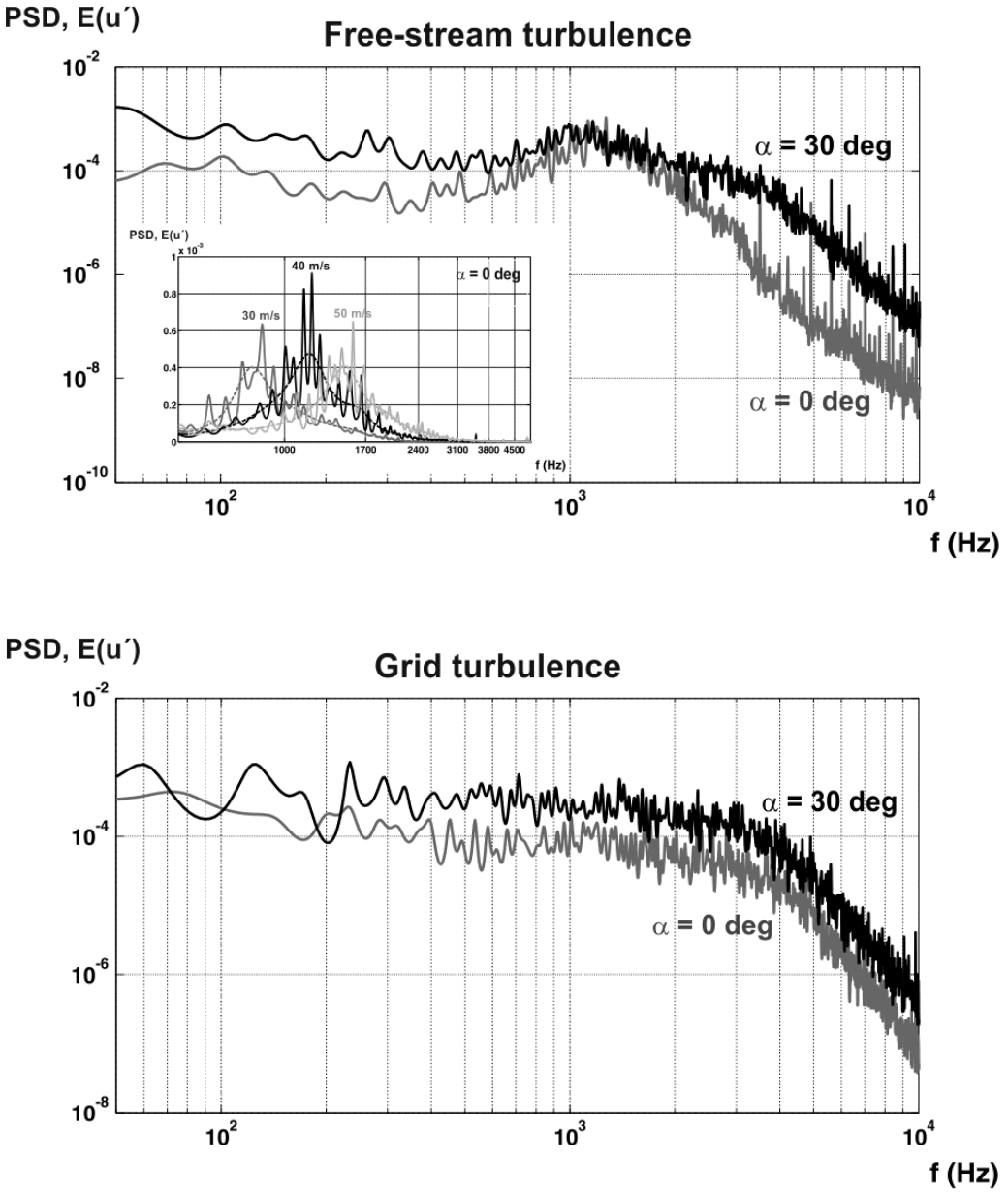

Fig. 8: Power spectrum density (PSD) of the axial velocity fluctuation (incident flow of 40 m/s). a) Free-stream turbulence conditions; b) Grid turbulence conditions.

Figure 9 shows the angular distribution of turbulence levels (in percentage) for the incident flow angle of 40 m/s. This intensity has been computed from the instantaneous fluctuation of the axial velocity. Note that these results are again free of errors from Reynolds number deviations. Whatever configuration considered, free-wake regions (from -40 to 0 deg) present quite uniform, low values, ranging between 1.5 and 2%. Conversely, from 0 deg on, due to the effect of interference, there is a significant increase in the turbulence intensity, reaching up to 3.5% for extreme angles of 40 deg. It is also remarkable the slight difference between turbulence levels for both datasets at free-wake regions, as a direct consequence of the extremely thin grid employed in these measurements.

These results confirm the overestimation in the measurement of the turbulence level when the probe is operated under wake-interference effects. Considering that hot-wire anemometry technique is widely used to characterize turbulent variables in real flows, it is quite reasonable to affirm that wake-affected regions are not valid ranges for measurements requiring high-frequency response.

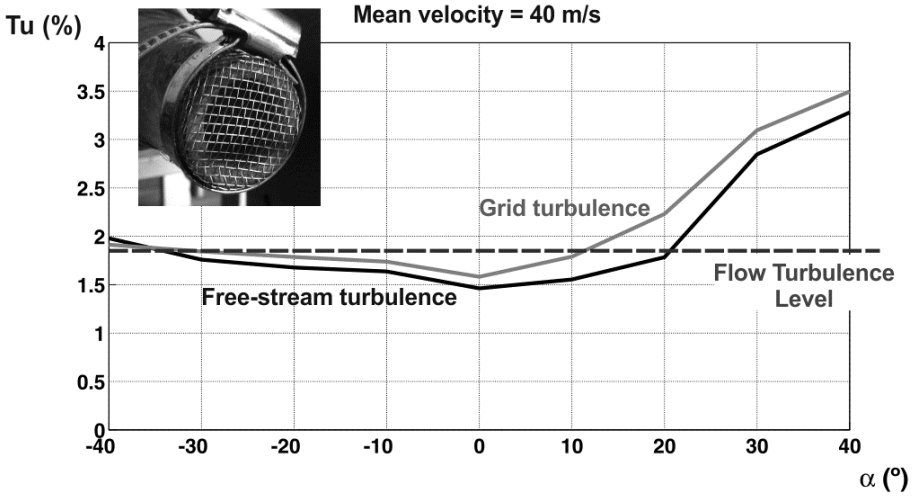

Fig. 9: Turbulence intensity as a function of the angular incidence (baseline conditions at 40 m/s).

Finally, figure 10 shows the effect of Reynolds number deviations from calibration conditions over the turbulence intensities measured from the instantaneous axial velocity. The shaded regions represent the angular distribution of the dispersion of the results, when reducing data with out-of-velocity calibrations, which somehow corresponds to the maximum associated errors. Dark grey band identifies the dispersion in the turbulence level estimation for the grid turbulence setting, while light grey band represents dispersion associated to free-stream conditions. Obviously, higher intensity levels throughout the whole angular range are obtained for the perturbed conditions of the grid turbulence setting. Dashed lines are turbulence intensity levels for the 50 m/s inlet flow, while solid lines represent those levels for the 30 m/s case. The overall trend is that when the mean velocity is increased, the turbulence level seems to be progressively reduced. For no interference zones, the evolution of the turbulence intensity is similar for all the considered velocities, with maximum discrepancies of a 0.5%. On the contrary, for wake-affected regions between 0 and 40 deg, changes in the intensity trends seem to be more pronounced with velocity variations, with typical errors in the order of 1%. Hence, it is not recommended the use of data obtained under wake interferences to characterize turbulence levels.

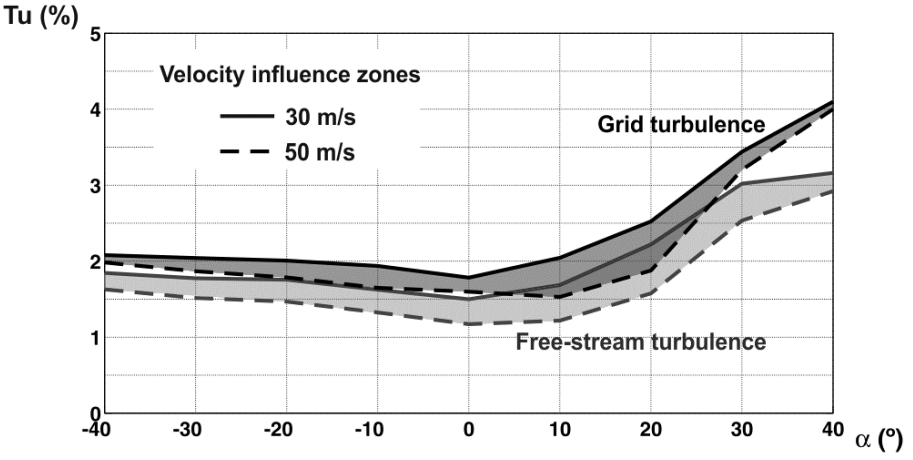

Fig. 10: Evolution of the turbulence intensity as a function of the probe yaw angle and deviations in the operative Reynolds number.

Calibration distributions of the Z-type and V-type probes (no wake effects of the prongs)

Following, figure 11 shows the angular distributions of the wire's output signals corresponding to the Z-type probe. As expected, there are no wake interference effects throughout the whole angular span. Only self-interactions with their own prongs arise, being more evident for both wires than in the case of the X-type probe. Such effects are observed at -75 and 80 deg for the first wire and around -22 and 135 deg for the second wire. Also, angular distributions for both wires are notably different between them, especially if they are compared with the results for the X-type probe.

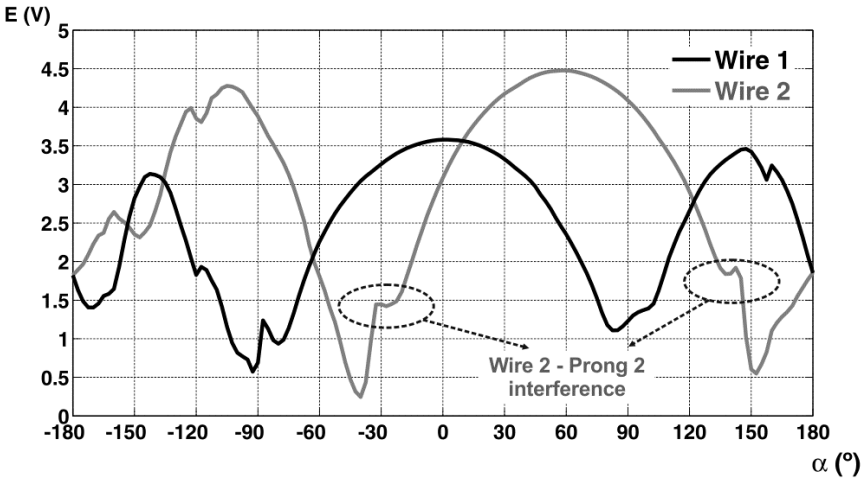

Fig. 11: Angular distributions of wires output voltage for a DHW Z-probe.

Additionally, figure 12 shows analogous results to figure 11, but now in the case of the V-type probe. Note that wake interference effects are missing again. The angular distribution for the outer wire is smoother than previous one for the Z-type, presenting less pronounced effects of self-interference which are now set off at 90 deg for wire 2 and -130 and 60 deg for wire 1.

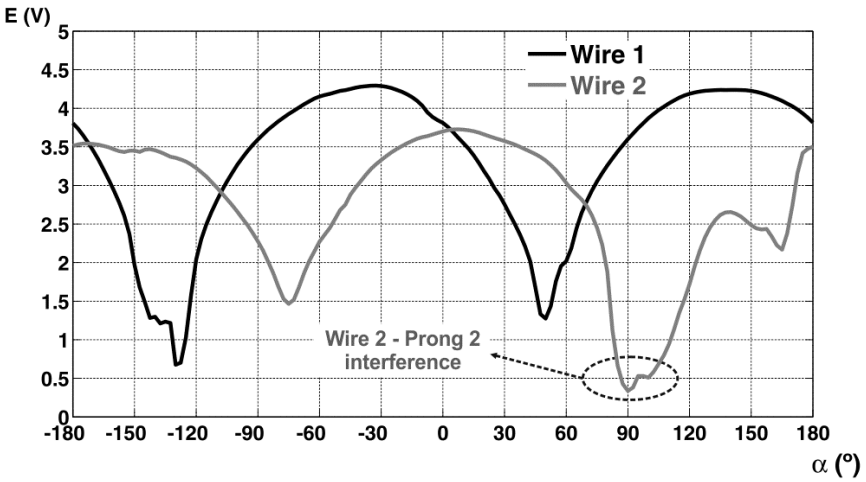

Fig. 12: Angular distributions of wires output voltage for a DHW V-probe.

Figure 13 represents the angular coefficients of both Z and V-type probes obtained after using equation 1. The angular range for the Z-type probe turns to be 102 deg, while the V-type is extended to 125 deg. In both cases, the significant increment in the operative angular range is a direct consequence of the absence of wake interference effects over the inner wire of the probes, as discussed in the introduction. For these free-wake

interference probes, the limitation in the angular range comes from the self-interaction of the wires with their own prongs. Therefore, it is reasonable to find a reduced angular range for the Z-type probe respect to the V-type because their self-interactions are more evident. The angular coefficient of the Z-type probe presents a higher slope than the one from the V-type, so it is presumable that the uncertainties and errors in the flow determination will be slightly higher in the case of the V-type probe.

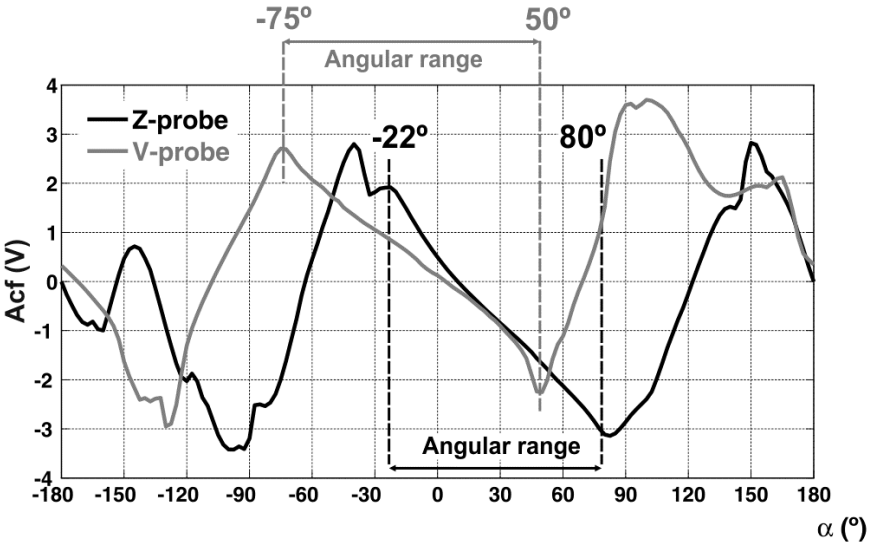

Fig. 13: Comparison of angular calibration coefficients for DHW Z- and V-probes.

Nevertheless, it can be assumed as a first approach that the angular distributions of the wires response are quite similar, so it is expected that both Z and V-type probes will provide identical results with comparable levels of error. The major difference would be placed in the operative angular range, 23 deg higher for the V-type. This fact, and the higher compactness and simplicity of V-type designs, makes them preferable to be manufactured and employed for measuring real flows.

CONCLUSIONS

In the present investigation, three different DHW probes have been manufactured and calibrated to analyze the impact of wake interference effects coming from adjacent prongs in the wire response of simple X-type probes. In particular, Z-type and V-type designs have been employed as free-wake interferences probes to quantify this detrimental phenomenon.

It has been confirmed that the existence of cross wire-prong interferences has a notable impact on the angular calibration of the probe and, therefore, in the accuracy of the measurements performed within real flows. For that purpose, the influence of these interferences on the errors associated to the retrievement of the flow angle and velocity magnitude when measuring at Reynolds numbers that differ notably from calibration conditions has been carried out.

Additionally, it has been explored the relevance of this effect over the determination of turbulent variables in DHW probes, which is really convenient since their high-frequency response is the strongest characteristic of these hot-wire anemometers.

Finally, it has been confirmed that these probe designs, manufactured without cross wire-prong effects, may present operative angular ranges up to 35 deg higher than classical X-type probes. This enhancement can be especially desirable for the characterization of unsteady flows with large angular variations (i.e. jet-wake patterns in turbomachinery environments). Besides, with these free-wake effects probes, the measurement errors associated to inaccuracies in the data reduction technique performed with calibration out of real flow conditions will be reduced.

REFERENCES

[1] Turan O and Azad RS. 1989. Effect of hot-wire probe defects on a new method of evaluating turbulence dissipation *J. Phys. E: Sci. Instrum*, **24**, 254–61.

[2] Cameron JD, Morris SC, Bailey S and smith A. 2010. Effects of hot-wire length on the measurement of turbulent spectra in anisotropic flows. *Meas. Sci. Technol*, **21**, 105407 (10 pp).

[3] Sanitjai S and Goldstein RJ. 2004. Forced convection heat transfer from a circular cylinder in crossflow to air and liquids. *International Journal of Heat and Mass Transfer*, **47**, 4795-4805.

[4] Jorgensen FE. 1996. The computer-controlled constant-temperature anemometer. Aspects of set-up, probe calibration, data acquisition and data conversion. *Meas. Sci. Technol*, **7**, 1378-1387.

[5] Freymuth P. 1977. Frequency response and electronic testing for constant-temperature hot-wire anemometers. *Journal of Physics E*, **10**, 705-710.

[6] Freymuth P. 1997. Interpretations in the control theory of thermal anemometers. *Meas. Sci. Technol*, **8**, 174-177.

[7] King LV. 1914. On the convection of heat from small cylinders in a stream of fluid: determination of the convection constants of small platinum wires with applications to hot-wire anemometry. *Philosophical Transactions of the Royal Society of London*, **214**, 373-432.

[8] Brunn HH, Khan MA, Al-Kayiem HH and Fardad AA. 1988. Velocity calibration relationships for hot-wire anemometry. *J. Phys. E: Sci. Instrum*, **21**, 225-232.

[9] Brunn HH. 1971. Interpretation of a hot-wire signal using a universal calibration law. *J. Phys. E: Sci. Instrum*, **4**, 225-232.

[10] Brunn HH and Tropea C. 1985. The calibration of inclined hot-wire probes. *J. Phys. E: Sci. Instrum*, **18**, 405-413.

[11] Blanco-Marigorta E, Ballesteros-Tajadura R and Santolaria C. 1998. Angular range and uncertainty analysis of non-orthogonal crossed hot wire probes. *Journal of Fluids Engineering*, **120**, 90-94.

[12] Stainback PC and Nagabushana KA. 1997. Review of hot-wire anemometry techniques and the range of their applicability for various flows. *Electronic Journal of Fluids Engineering*, **119**.

[13] Lekakis I. 1996. Calibration and signal interpretation for single and multiple hot-wire/hot-film probes. *Meas. Sci. Technol*, **7**, 1313-1333.

[14] Brunn HH, Nabhani N, Al-Kayiem HH, Fardad AA, Khan MA and Hogarth E. 1990. Calibration and analysis of X hot-wire probe signals. *Meas. Sci. Tecnol*, **1**, 782-785.

[15] Brunn HH, Nabhani N, Fardad AA and Al-Kayiem HH. 1990. Velocity component measurements by X hot-wire anemometry. . *Meas. Sci. Tecnol*, **1**, 1314-1321.

[16] Comte-Bellot G, Strohl A and Alcaraz E. 1971. On aerodynamic disturbances caused by single hot-wire probes. *J. Appl. Mech*, **38**, 767-774.

[17] Strohl A and Comte-Bellot G. 1973. Aerodynamic effects due to configuration of X-wire anemometers. *J. Appl. Mech*, **40**, 661-666.

[18] Adrian RJ, Johnson RE, Jones BG, Merati P and Tung ATC. 1984. Aerodynamic disturbances of hot-wire probes and directional sensitivity. *J. Phys. E: Sci. Instrum*, **17**, 62-71.